Observational characteristics of the tropopause inversion layer derived from CHAMP/GRACE radio occultations and MOZAIC aircraft data

T. Schmidt, Jean-Pierre Cammas, H. G. J. Smit, S. Heise, J. Wickert, A. Haser

Observational characteristics of the tropopause inversion layer derived from CHAMP/GRACE radio occultations and MOZAIC aircraft data

T. Schmidt,[1] J.-P. Cammas,[2] H. G. J. Smit,[3] S. Heise,[1] J. Wickert,[1] and A. Haser[1]

Received 30 March 2010; revised 5 October 2010; accepted 15 October 2010; published 16 December 2010.

[1] In this study we discuss characteristics of the Northern Hemisphere (NH) midlatitude (40°N–60°N) tropopause inversion layer (TIL) based on two data sets. First, temperature measurements from GPS radio occultation data (CHAMP and GRACE) for the time interval 2001–2009 are used to exhibit seasonal properties of the TIL bottom height defined here as the height of the squared buoyancy frequency minimum N^2 below the thermal tropopause, the TIL maximum height as the height of the N^2 maximum above the tropopause, and the TIL top height as the height of the temperature maximum above the tropopause. Mean values of the TIL bottom, TIL maximum, and TIL top heights relative to the thermal tropopause for the NH midlatitudes are (−2.08 ± 0.35) km, (0.52 ± 0.10) km and (2.10 ± 0.23) km, respectively. A seasonal cycle of the TIL bottom and TIL top height is observed with values closer to the thermal tropopause during summer. Secondly, high-resolution temperature and trace gas profile measurements on board commercial aircrafts (Measurement of Ozone and Water Vapor by Airbus In-Service Aircraft (MOZAIC) program) from 2001–2008 for the NH midlatitude (40°N–60°N) region are used to characterize the TIL as a mixing layer around the tropopause. Mean TIL bottom, TIL maximum, and TIL top heights based on the MOZAIC temperature (N^2) measurements confirm the results from the GPS data, even though most of the MOZAIC profiles used here are available under cyclonic situations. Further, we demonstrate that the mixing ratio gradients of ozone (O_3) and carbon monoxide (CO) are suitable parameters for characterizing the TIL structure.

Citation: Schmidt, T., J.-P. Cammas, H. G. J. Smit, S. Heise, J. Wickert, and A. Haser (2010), Observational characteristics of the tropopause inversion layer derived from CHAMP/GRACE radio occultations and MOZAIC aircraft data, *J. Geophys. Res.*, *115*, D24304, doi:10.1029/2010JD014284.

1. Introduction

[2] The tropopause inversion layer (TIL) is a region of enhanced static stability about 1–2 km above the first lapse rate tropopause (LRT) and is present during all seasons and occurs in nearly all geographical regions, mainly in the extratropics, but also in the tropics. The TIL as a permanent property of the extratropical tropopause region is a relatively new feature and was discovered by *Birner* [2006]. His results are based on the analysis of high-resolution radiosonde data from Germany and the United States where the usage of a tropopause-based coordinate system was the base for the detection of the persistent inversion layer just above the LRT height.

[3] This region of enhanced static stability which is usually expressed by the square of the buoyancy frequency N has been a focus of interest [*Randel et al.*, 2007; *Hegglin et al.*, 2009; *Kunz et al.*, 2009; *Grise et al.*, 2010; *Randel and Wu*, 2010]. Formation mechanisms of the TIL are still a subject of investigation and not finally clarified yet. At the moment, there are two main models under discussion. *Birner* [2006], *Wirth and Szabo* [2007] (but already *Wirth* [2003]) and *Son and Polvani* [2007] explain the existence of the TIL due to dynamical processes, whereas *Randel et al.* [2007] and *Randel and Wu* [2010] argue that the maintenance of the TIL is mainly driven by radiative processes due to the strong gradients of water vapor and ozone across the tropopause.

[4] The global behavior of the TIL can only be observed with high vertical resolution temperature data from satellites. Global Positioning System (GPS) radio occultation (RO) enables atmospheric information with relatively high vertical resolution (~100 m in the tropopause region). The GPS RO technique requires no active calibration, it is weather independent, and the occultations are almost uniformly distributed over the globe [*Melbourne et al.*, 1994; *Kursinski et al.*, 1997].

[1] Helmholtz Centre Potsdam, GFZ German Research Centre for Geosciences, Potsdam, Germany.
[2] Laboratoire d'Aerologie, Observatoire Midi-Pyrénées, CNRS, Toulouse, France.
[3] Institute for Energy and Climate Research: Troposphere, Research Centre Jülich, Jülich, Germany.

0148-0227/10/2010JD014284

[5] With the German CHAMP (CHAllenging Minisatellite Payload) satellite launched in July 2000 the first RO experiment providing data continuously in an operational manner between May 2001 and September 2008 [*Wickert et al.*, 2001, *Schmidt et al.*, 2005a] was started. Since 2006 the U.S.-German GRACE (Gravity Recovery And Climate Experiment) satellite continues this first long-term RO data set [*Wickert et al*, 2009]. Further RO missions whose data are not considered in this study are the six-satellite COSMIC (Constellation Observing System for Meteorology, Ionosphere, and Climate) constellation (since 2006), the European Metop mission (since 2006) and the German TerraSAR-X (since 2007) satellite.

[6] The accuracy of the RO temperature measurements could be broadly documented. In the past, several comparison studies between GPS RO data and radiosondes as well as cross validations with other satellite sensors have been performed [*Hajj et al*, 2004; *Kuo et al.*, 2005; *Steiner et al.*, 2007; *Gobiet et al.*, 2007; *Schmidt et al.*, 2008; *Heise et al.*, 2008]. Special comparisons of tropopause parameters between CHAMP and ECMWF (European Centre for Medium-Range Weather Forecasts) or NCEP (National Centers for Environmental Prediction) analyses are given by, for example, *Borsche et al.* [2007] and *Schmidt et al.* [2004, 2005b].

[7] *Grise et al.* [2010] give a survey of static stability using CHAMP RO data from 2002–2008. The authors discuss detailed global climatological features of the static stability (N^2), and the study can be considered as the most comprehensive publication on that topic to date.

[8] Summarizing the results from previous investigations [e.g., *Birner et al.*, 2006; *Randel et al.*, 2007; *Hegglin et al.*, 2009; *Grise et al.*, 2010; *Randel and Wu*, 2010] the main observational features of the extratropical TIL in terms of the square of the buoyancy frequency N are: (1) the local minimum of N^2 about 2 km below the thermal tropopause height (TPH), (2) the maximum of N^2 just above the thermal TPH, (3) the temperature maximum (inversion) in a layer 2–3 km above the thermal TPH, and (4) the local minimum of N^2 about 3–4 km above the thermal TPH.

[9] According to mean N^2 profiles, *Hegglin et al.* [2009] consider the local minimum of N^2 below the LRT as the bottom of the TIL and the local minimum of N^2 above the LRT as the top of the TIL. We use this nomenclature also in this study and link the expression "TIL bottom height" to the height of the local minimum of N^2 below the LRT. For the height of N^2 maximum above the LRT the expression "TIL maximum height" is introduced, whereas we define the TIL top height here as the height of the temperature maximum above the tropopause (the maximum inversion layer). The TIL top height based on our definition is comparable with the upper border of highest static stability ($N^2 > 5{\cdot}10^{-4}$ s^{-2}) above the LRT [*Kunz et al.*, 2009].

[10] The TIL heights are part of the upper troposphere and lower stratosphere region where the chemical transition and exchange between both parts of the atmosphere take place with fundamental impacts to the radiative balance. As demonstrated, for example, by *Pan et al.* [2004] the extratropical tropopause transition layer (ExTL) is centered around the thermal tropopause with a thickness of about 2–3 km. Following the argumentation suggested from *Randel et al.* [2007] the forcing and maintenance of the TIL is caused by radiative effects of ozone and water vapor near the tropopause while ozone acts to warm the layer above the tropopause and water vapor acts in the other direction and cools the tropopause. An important point in that argumentation is the fact that ozone and water vapor are mixed [*Kunz et al.*, 2009]. Therefore the consideration of the extratropical TIL as a mixing layer around the tropopause or as part of the ExTL is an important issue.

[11] *Hegglin et al.* [2009] have shown the usefulness of trace gas mixing ratio gradients from ACE-FTS (Atmospheric Chemistry Experiment Fourier Transform Spectrometer) on board the Canadian SCISAT-1 satellite mission between 2004 and 2007 for the characterization of the ExTL. The authors show also a similar structure of the relative vertical water vapor gradients for summer and winter months compared with the mean N^2 structure that *Randel et al.* [2007] found from GPS RO data. This results support the radiative-driven mechanism for the TIL maintenance.

[12] *Kunz et al.* [2009] provide further support for the radiative-based explanation from observations of SPURT (trace gas transport in the tropopause region) ozone and carbon monoxide aircraft measurements. They reported highest mixing in the TIL correlated with high N^2 values ($N^2 > 5{\cdot}10^{-4}$ s^{-2}).

[13] In this study we analyze the Northern Hemisphere (NH) midlatitude (40°N–60°N) TIL structure based on temperature and N^2 from GPS RO data (2001–2009) and compare the results with high-resolution temperature measurements and N^2 from MOZAIC data for the same latitude band.

[14] MOZAIC stands for Measurement of Ozone and Water Vapor by Airbus In-Service Aircraft [*Marenco et al.*, 1998; *Thouret et al.*, 1998a, 1998b] was launched in 1993 and is still active. Several European commercial airliners (Airbus A340) are equipped with automatically measuring instruments to tape ozone, water vapor, carbon monoxide, and other trace gases on their regularly flights between Europe and several regions worldwide (mainly to North America and East Asia). In this study we use the recorded profile measurements during takeoff and landing for the time interval from May 2001 (start of the RO measurements) and 2008 (profile data from the MOZAIC data base at http://mozaic.aero.obs-mip.fr/extract).

[15] The ozone (O_3) and carbon monoxide (CO) measurements are used additionally to characterize the vertical structure of the TIL. We demonstrate that the climatological TIL structure observed in N^2 from RO and MOZAIC is also present in the mixing ratio gradients of O_3 and CO.

[16] By defining simple threshold values for the different trace gas mixing ratio gradient profiles from MOZAIC, we are able, at least in a climatological sense, to reproduce the local minimum of N^2 below the LRT (TIL bottom height) with O_3 gradients and the maximum of N^2 above the LRT (TIL maximum height) with CO gradients. The threshold values are based on the typical mean characteristics of the according trace gas gradient profiles.

[17] Further, we show that the height of the absolute maximum (minimum) of the mixing ratio gradients in an ozone (carbon monoxide) profile agrees with the height of the LRT, at least statistically.

[18] This leads to the definition of so-called trace gas tropopauses and we introduce the following abbreviations here: TPH_{Ozone} as the ozone tropopause height and TPH_{CO} as the carbon monoxide tropopause height.

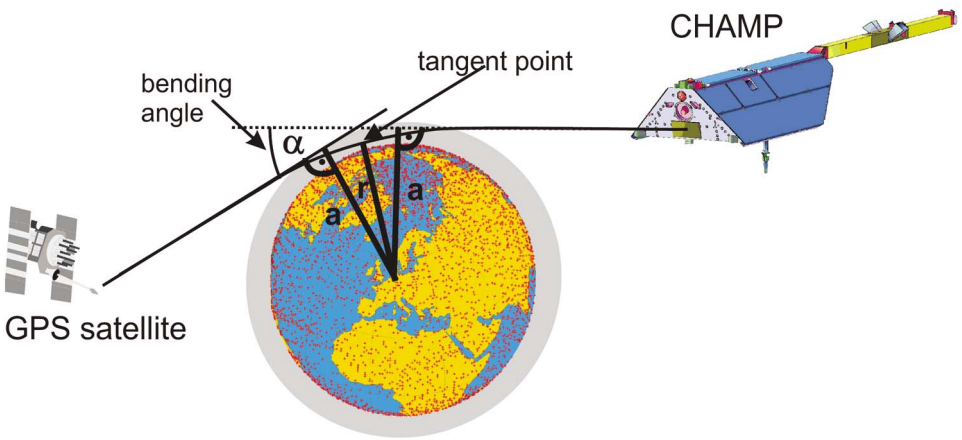

Figure 1. Principle of the GPS radio occultation technique.

[19] The LRT is determined from the MOZAIC temperature measurements itself. Applying the *World Meteorological Organization (WMO)* [1957] definition of the thermal tropopause, only profiles that reach a top altitude of at least LRT +2 km can be considered. The flight level of commercial airliners is between 9 and 12 km, but midlatitude tropopause heights can also be higher than that altitude. Therefore only cases with relatively low tropopauses can be considered here which are mainly associated with cyclonic conditions or upper level troughs [*Wirth*, 2001, 2003; *Randel et al.*, 2007; *Brioude et al.*, 2008].

[20] *Randel et al.* [2007] have shown with GPS RO data that the highest stability occurs during anticyclonic cases, but the mean structure of the N^2 profiles is preserved during cyclonic, anticyclonic or near-zero cases. This means that the relative TIL heights are nearly unchanged between the different synoptic situations. The TIL structure derived from the more cyclonic affected MOZAIC cases is discussed in section 4.2.

[21] As already mentioned, we use the local thermal tropopause here and relate our results to that altitude because high-resolution temperature measurements from MOZAIC are available in parallel to the O_3 and CO measurements. This is a big advantage of the MOZAIC profile data set compared with other.

[22] On the other hand, the dynamical tropopause based on potential vorticity (PV) surfaces has advantages for investigations of stratosphere-troposphere exchange. Under adiabatic conditions the PV is a conservative stratosphere tracer and the PV-based tropopause can be used to locate the surface that indicate the chemical transition from the stratosphere to the troposphere [*Holton et al.*, 1995]. Nevertheless, we use the thermal tropopause here also with regard to comparisons of the N^2 structure between GPS RO and MOZAIC results.

[23] The paper is structured as follows. In section 2 the different data sets (RO and MOZAIC data) and methods, for example, the derivation of the LRT, the static stability, and the trace gas mixing ratio gradients, are described. In section 3 the synoptic situation with respect to cyclonic/anicyclonic situations near the tropopause level is reported. Section 4 gives an overview of global N^2 observations from CHAMP/GRACE and MOZAIC data, whereas in section 5 the MOZAIC trace gas measurements and the usage of their mixing ratio gradients for the representation of the TIL structure is discussed.

2. Data and Methods

2.1. GPS Radio Occultation Data

[24] The CHAMP mission has generated the first long-term GPS RO data set (2001–2008). Besides one complete month of missing data (July 2006), CHAMP delivered continuously between 150 and 200 temperature profiles daily. To continue the CHAMP data set ending in September 2008 and additionally to the CHAMP data since 2006, we use RO data from GRACE-A (between April 2006 and October 2009) delivering atmospheric profiles with the same daily data rate. The GRACE GPS receiver and error characteristics are comparable with CHAMP [*Wickert et al.*, 2009].

[25] The RO technique is described here briefly: The GPS receiver on board a low Earth orbiting (LEO) satellite records phase and amplitude variations with high temporal resolution (e.g., 50 Hz) during an occultation event (Figure 1). By using high-precision orbit information from the LEO and the occulting GPS satellite the atmospheric excess phase can be extracted which is related to a bending angle profile α as a function of the impact parameter a.

$$a = nr = n(z + R_c) \tag{1}$$

(n: refractive index, r: tangent radius, z: geometric height, and R_c: local radius of curvature).

[26] Assuming spherical symmetry the bending angles can be related to the refractive index n using an Abel transformation. Finally, the atmospheric refractivity N_{ref} is given after *Smith and Weintraub* [1953]

$$N_{ref} = (n-1)\cdot 10^6 = 77.6\frac{p}{T} + 3.73\cdot 10^5 \frac{e_w}{T^2} \tag{2}$$

(p: total air pressure, T: air temperature, and e_w: water vapor pressure).

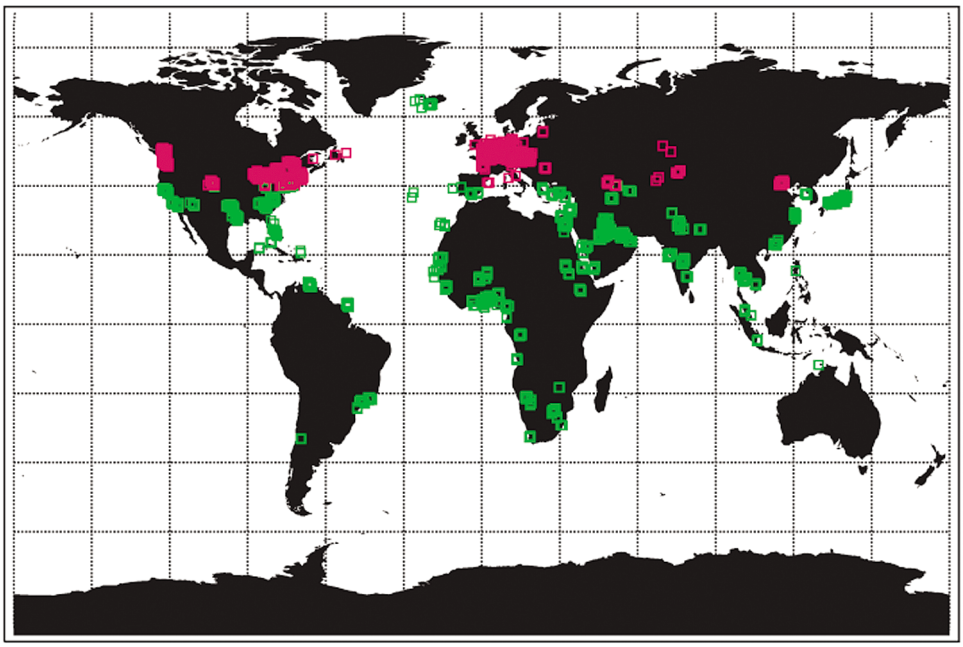

Figure 2. Locations of the atmospheric profiles from the MOZAIC aircraft measurements between 2001 and 2008. The locations are averages of the first and last latitude/longitude positions of the profile data. Red color indicates data for 40°N–60°N used in this study.

[27] To convert the refractivity profiles into pressure and temperature profiles the assumption of dry air has to be made because of the ambiguity between the dry and wet part in the resulting refractivity (equation (2)). Further on, by applying the hydrostatic equation, pressure and temperature profiles can be calculated. In the current retrieval version 005 [*Wickert et al.*, 2009] ECMWF pressure at 43 km is used for the initialization of an iteration for the pressure profile. This is one atmospheric scale height above the upper level for which profile data are provided (35 km) from GFZ.

[28] The physical vertical resolution of RO measurements depends on implemented retrieval algorithms. In our current software version a vertical resolution of less than 100 m up to 15 km is given; above 15 km altitude the vertical resolution increases up to about 1–1.5 km between 30 and 35 km. For data provision all data were sampled on a 200 m grid between the lowest available level and 35 km.

2.2. MOZAIC Aircraft Measurements

[29] The MOZAIC program was initiated in 1993 with the goal to collect experimental data on atmospheric composition and to observe its changes with particular interest in the effects of aircrafts [*Marenco et al.*, 1998]. For this reason, long-range airliners are equipped with instruments able to perform in situ measurements of O_3, H_2O, CO and nitrogen oxides (NO_y).

[30] The following airlines attend to the MOZAIC program: one Airbus from Air France and Austrian between August 1994 and 2005, two Airbus from Lufthansa since August 1994, and one Airbus from Air Namibia between January 2005 and July 2009 (as of November 2009; http://mozaic.aero.obs-mip.fr/web/features/news.html).

[31] MOZAIC observations are available since mid-1994 and cover large parts of Europe, North America, and East Asia, but also regions in Africa and South America. The measurements of each flight are divided into three sets: ascent, cruise, and descent. In this study we use only the profile data (ascent or descent) of all flights performed between May 2001 and December 2008. A total number of 28,770 profiles are available for the time interval (Figure 2). The locations of the measurements in Figure 2 are averages of the first and last latitude/longitude positions of the reported start or end of the profile.

[32] The time interval chosen here starts with the beginning of RO measurements from CHAMP and ends with the data available in the MOZAIC data base (mozaic.aero.obs-mip.fr/extract) whereas the availability of O_3 and CO profile data is different (O_3 data from May 2001 to December 2008; CO data from January 2002 to December 2008).

[33] The MOZAIC raw data are delivered with a 4 s time resolution equivalent to a vertical resolution of about 30 m. The ozone instrument has a 4 s response time (~30 m vertical resolution) and the accuracy is estimated at ±2 ppbv (±2%) [*Thouret et al.*, 1998a]. The CO instrument has a 30 s response time (~300 m vertical resolution) and an accuracy of about ±5 ppbv (±5%) [*Nedelec et al.*, 2003].

[34] The MOZAIC temperature used here is the static temperature, i.e., the temperature of the undisturbed ambient air through which the aircraft is about to fly measured with a platinum resistance sensor PT100 [*Marenco et al.*, 1998; *Helten et al.*, 1998].

[35] Raw data of the ascent and descent profiles are averaged on a fixed altitude grid of 85 layers, each 150 m thick. These midlayer altitudes are constant for all profiles.

2.3. Methods

2.3.1. Lapse Rate Tropopause Heights

[36] The definition of the lapse rate tropopause [*WMO*, 1957] was applied to each individual GPS RO temperature profile from CHAMP/GRACE and MOZAIC between

Table 1. Number of Northern Hemisphere Midlatitude (40°N–60°N) MOZAIC Profiles With Different Characteristics[a]

	Total Number	Number of LRT	
		WMO	Modified
All profiles	18,895		
Max. height >5 km	18,560		
Max. height >6 km	18,537		
Max. height >7 km	18,484		
Max. height >8 km	18,417		
Max. height >9 km	16,784		
Max. height >10 km	11,250		
Max. height >11 km	7808		
Max. height >12 km	835		
LRT identified		1088	3049
LRT height >6 km		1088	3049
LRT height >7 km		1031	2987
LRT height >8 km		857	2773
LRT height >9 km		473	2197
LRT height >10 km		32	1160
LRT height >11 km		0	81
LRT and O_3 data		830	2303
LRT and CO data		749	not used
LRT, O_3 and CO data		647	not used

[a]LRT denotes the lapse rate tropopause.

450 hPa and 70 hPa to determine the first LRT, whereas the tropopause algorithm from *Reichler et al.* [2003] was used.

[37] For validation purposes (see below), LRT heights were also determined from 6-hourly ECMWF operational analyses interpolated to the time and location of the MOZAIC profiles. The ECMWF data used here have a horizontal resolution of ~0.5 deg (reduced Gaussian grid N160) and a vertical resolution of ~0.8 km in the tropopause region (60 model level until January 2006; 91 model level after).

[38] One can recognize from Table 1 that in only 6% of all MOZAIC profiles between 40°N and 60°N a LRT can be identified applying the WMO criterion. This data amount is further reduced if we only consider profiles with an identified LRT and additional O_3 and CO data (bottom rows in Table 1).

[39] The *WMO* [1957] defines the LRT as "the lowest level at which the lapse rate decreases to 2°C/km or less, provided that the averaged lapse rate between this level and all higher levels within 2 km does not exceed 2°C/km." To increase the amount of data for the N^2 statistics especially below the tropopause, but also in the first kilometers above the tropopause (where the TIL maximum height is located), the WMO criterion was modified to be less restrictive: a LRT is also detected if the last point of the profile is between 1 and 2 km above a possible tropopause; that is, the strong 2 km criterion was modified.

[40] Figure 3 shows an example for a detected LRT applying the WMO criterion. In the modified version the LRT would also be valid if the difference between the last MOZAIC data point and the LRT is at least 1 km.

[41] It should be noted that the following results concerning the TIL structure are based on MOZAIC profiles with O_3 and CO data and a LRT deduced with the strong WMO criterion. Results based on tropopauses deduced with the modified WMO criterion will be indicated.

[42] In Figure 3 also a colocated ($\Delta t < 3$ h and $\Delta d <$ 300 km; t = time, d = distance) GPS RO temperature profile is included, demonstrating a good agreement.

2.3.2. Validation

[43] A comparison of the thermal tropopauses derived from MOZAIC temperature profiles and ECMWF dependent on the difference between the last MOZAIC profile height and the LRT is presented in Figure 4a. The data points within the red window (1088) show the bias between the MOZAIC tropopause heights (TPH_{MOZAIC}) and the ECMWF tropopause heights (TPH_{ECMWF}) applying the strong WMO criterion. The mean bias of 30 m (standard deviation of 740 m) demonstrates the good agreement. Applying the modified WMO criterion an even better result (zero bias) is achieved.

[44] Figure 4b shows as an additional validation the LRT height bias between nearby located MOZAIC and GPS RO measurements and ECMWF (61 cases). Mean LRT height biases between MOZAIC and GPS RO (ECMWF) tropopauses of −90 m (40 m) are observed with a higher standard deviation between MOZAIC-GPS RO compared with MOZAIC and ECMWF.

[45] It should also be noted that for the GPS RO and ECMWF tropopauses in Figure 4 the strong WMO criterion was applied.

2.3.3. Static Stability

[46] As mentioned above the static stability is expressed as the square of the buoyancy frequency N given by

$$N^2 = \frac{g}{T} \cdot \left(\Gamma + \frac{\partial T}{\partial z} \right) \tag{3}$$

(g = 9.80665 m/s^2: acceleration due to gravity; T: temperature; Γ = 0.0098 K/m: dry adiabatic temperature gradient; $\partial T/\partial z$: temperature gradient).

[47] For the temperature gradients, simple forward differences of the according CHAMP/GRACE or MOZAIC temperature profiles were applied. Mean values of N^2 in the troposphere and lower stratosphere are $1{\cdot}10^{-4}$–$2{\cdot}10^{-4}$ s^{-2} and $4{\cdot}10^{-4}$–$5{\cdot}10^{-4}$ s^{-2} [*Andrews et al.*, 1987] (see also section 4.1).

[48] A detailed discussion of the static stability with respect to the seasonal cycle in different regions, the longitudinal

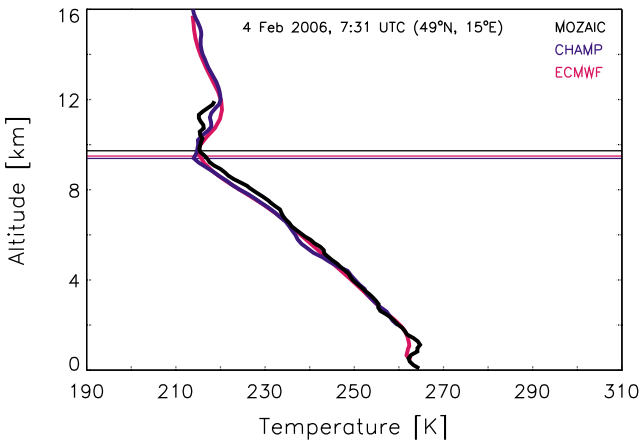

Figure 3. Examples for nearby MOZAIC and CHAMP temperature profiles and ECMWF. The horizontal lines denote the according lapse rate tropopause.

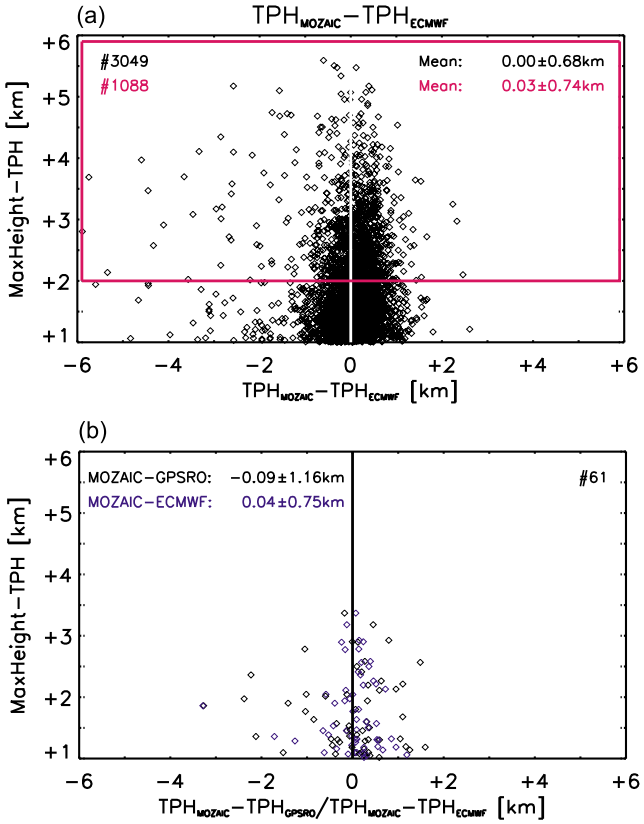

Figure 4. (a) Comparison of MOZAIC lapse rate tropopause (LRT) heights with ECMWF in relation to the difference between the last MOZAIC data point (MaxHeight) and the LRT. The LRT for data within the red window were determined using the strong WMO criterion, and all other LRTs used the modified WMO version. For further explanation, see text. (b) Comparison of nearby MOZAIC and GPSRO LRTs (black) and MOZAIC and ECMWF (blue).

structure, and stratospheric processes associated with the variability of the TIL are given by *Grise et al.* [2010].

3. MOZAIC Data and the Synoptic Situation

[49] Because of the mean flight ceiling of commercial aircrafts between 9 and 12 km the number of MOZAIC profiles with an identified thermal tropopause following the WMO criterion is limited (see Table 1).

[50] The global mean LRT height between 40°N and 60°N based on GPS RO data for the time interval May 2001 and December 2008 is about 10.5 km. The MOZAIC profiles for the same time interval used here give a mean LRT height of (8.75 ± 0.85) km, whereas the mean LRT deduced with the modified WMO criterion is accounted for (9.56 ± 0.99 km). The values are 1.8 km and 1.0 km below the LRT derived from GPS RO. As already mentioned above, low tropopauses are mostly associated with cyclonic or upper-level trough situations [*Wirth*, 2003; *Randel et al.*, 2007; *Brioude et al.*, 2008].

[51] *Randel et al.* [2007] have demonstrated the relation between mean N^2 and cyclonic/anticyclonic situations using the relative vorticity ξ at 200 hPa. Their results show that the tropopause inversion is little stronger for anticyclonic situations, but also present under cyclonic flow. The N^2 maximum just above the thermal tropopause is also highest for anticyclonic cases compared with the cyclonic ones and the tropospheric N^2 is lowest for anticyclonic conditions, but the structure of the mean N^2 profiles for the different situations is similar; that is, the TIL bottom and TIL maximum heights are unchanged.

[52] For the classification of cyclonic or anticyclonic situations of the MOZAIC profile measurements, we follow the suggestion from *Randel et al.* [2007] and define cyclonic situations with a relative vorticity $\xi > 3 \cdot 10^{-5}$ s^{-1} and anticyclonic cases with $\xi < -3 \cdot 10^{-5}$ s^{-1}. All situations between this values are called near-zero cases.

[53] We use the relative vorticity at 200 hPa from ECMWF (ERA interim) data (0.5 deg horizontal resolution) interpolated to the time and location of the MOZAIC profiles.

[54] In Figure 5 the time series of the relative vorticity to the appropriate MOZAIC profiles with LRT heights following the strong (Figure 5a) and modified (Figure 5d) WMO criterion is presented. The relative frequency distribution (Figure 5b) show the strong cyclonic influence for profiles with tropopauses derived after the strong WMO criterion. The dominant number of measurements during December–February (DJF) and March–May (MAM) is evident. This is due to the fact that the thermal tropopause is on average lower during winter compared with summer and the flight ceiling of the aircrafts is above the tropopause level.

[55] The modified alternative of the tropopause determination includes more near-zero cases, but anticyclonic situations are also very rare (Figure 5e).

[56] The scatterplots of LRT height versus relative vorticity (Figures 5c and 5f) demonstrate that the MOZAIC tropopauses do not exceed 11 km.

4. Global N^2 Observations

4.1. CHAMP/GRACE

[57] Before describing the TIL structure derived from MOZAIC profiles a short global overview of the seasonal N^2 distribution is given using the GPS RO data from CHAMP and GRACE. Similar work was already done by *Randel et al.* [2007] and *Grise et al.* [2010], but our focus here is more the discussion of the mean TIL heights (bottom, maximum and top) which we relate to the MOZAIC O_3 and CO gradients (see section 5).

4.1.1. Individual Profiles

[58] Figures 6a and 6b shows examples of tropical and midlatitude GRACE temperature profiles measured in January and July 2009. The vertical coordinate here and for the following plots is centered at the LRT and individual properties are shown ±6 km (or ±10 km) around the thermal tropopause. Nearly all temperature profiles exhibit a more or less strong inversion just above the LRT which is a characteristic for the TIL.

[59] The associated N^2 profiles (Figures 6c and 6d) represent a relative maximum within 1–2 km above the LRT [see also *Randel et al.*, 2007; *Grise et al.*, 2010]. This maximum height is clearly pronounced in the midlatitude examples and also visible in the tropics, but more scattered there.

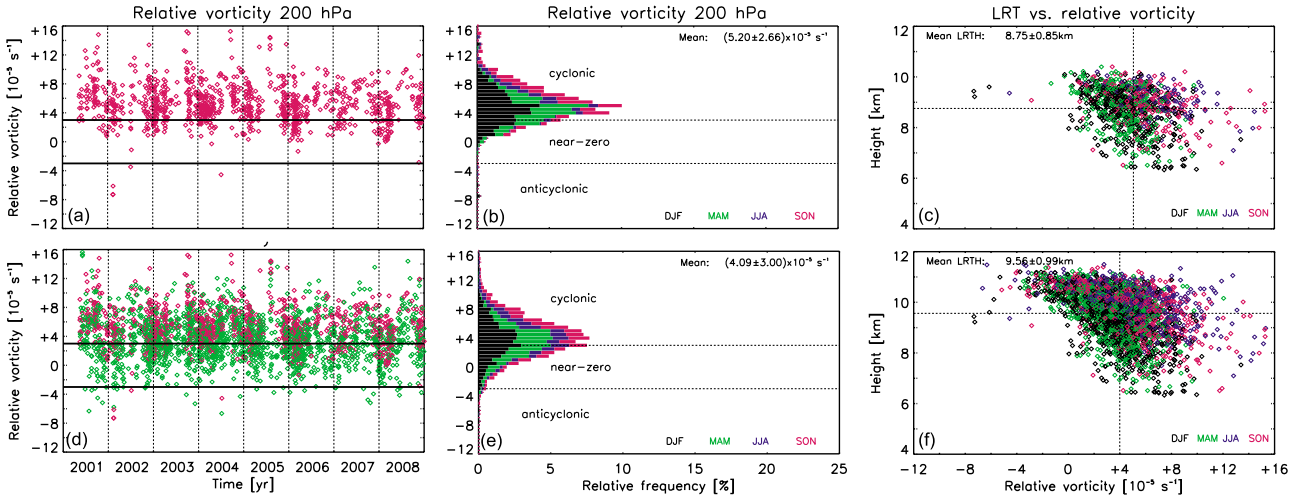

Figure 5. (a) Time series of relative vorticity at 200 hPa from ERA interim interpolated to the time and location of MOZAIC measurements. (b) Frequency distribution of the data from Figure 5a for different seasons (DJF, December–February; MAM, March–May; JJA, July–August; SON, September–November). (c) Scatterplot of MOZAIC lapse rate tropopauses versus relative vorticity. The horizontal line denotes the mean tropopause height. The vertical line represents the mean relative vorticity. For Figures 5a–5c the strong WMO criterion was used. (d–f) Same as Figures 5a–5c but for the application of the modified WMO criterion. In Figure 5d, red is strong WMO criterion and green is modified WMO criterion.

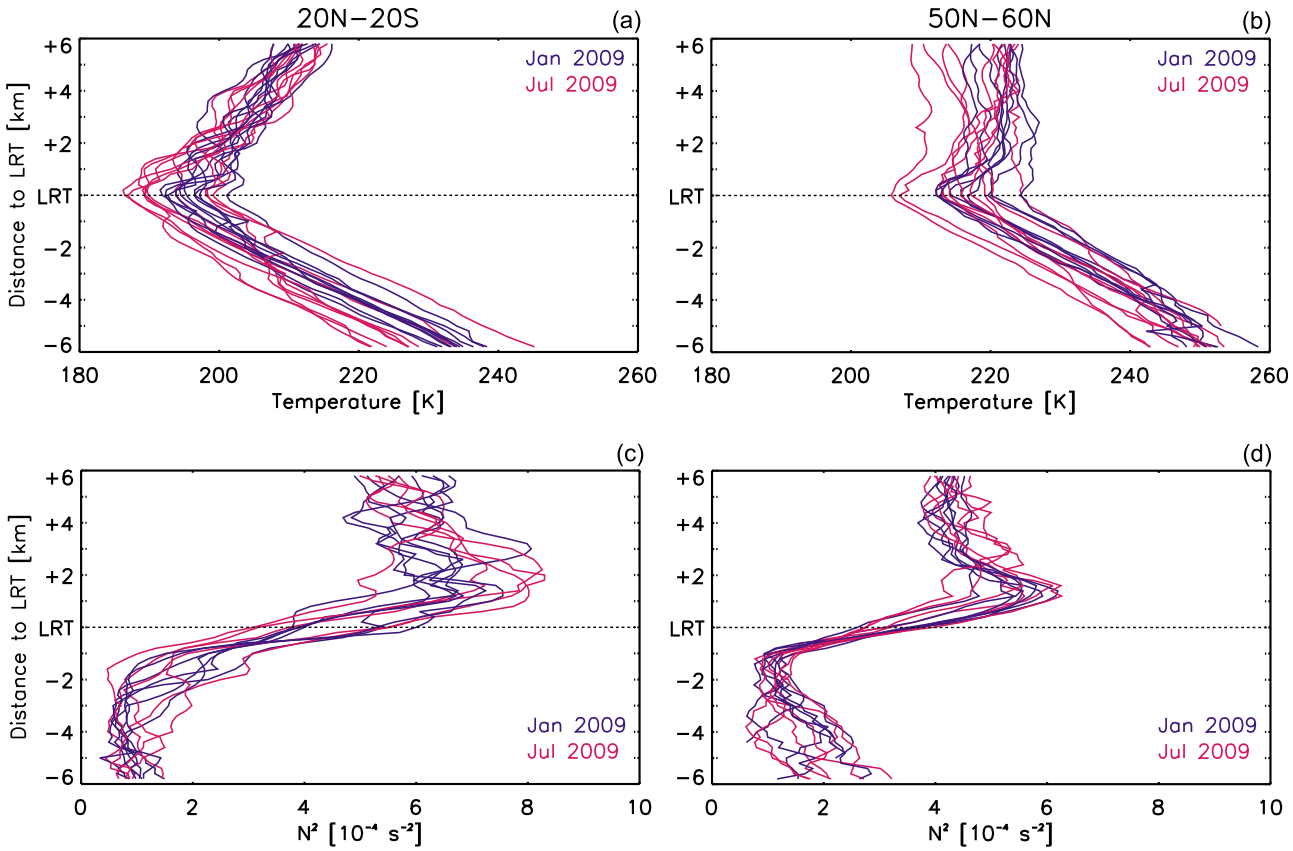

Figure 6. Examples of (a, b) individual temperature and (c, d) N^2 profiles from GRACE for the tropics (Figures 6a and 6c) and midlatitudes (Figures 6b and 6d) for January (blue) and July (red) 2009. The vertical coordinate is tropopause-based.

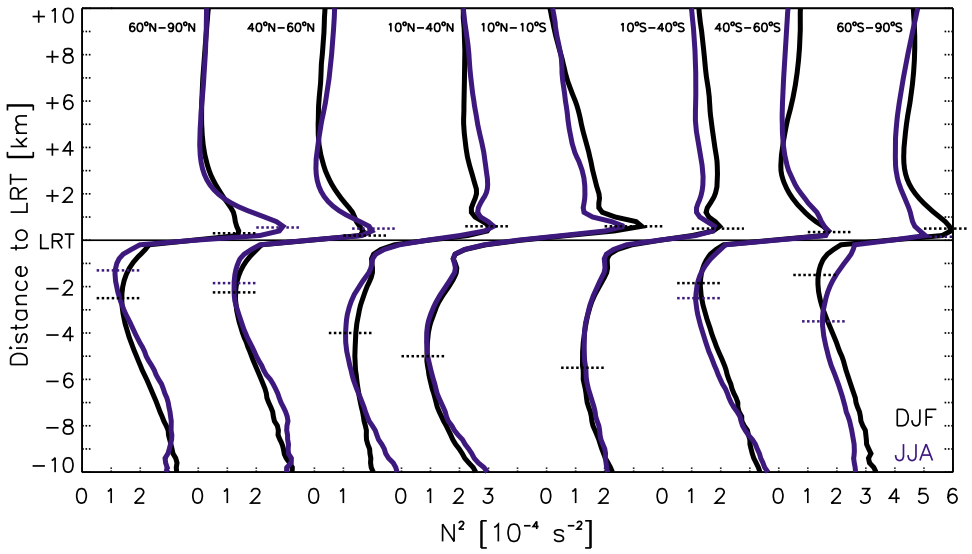

Figure 7. Mean N^2 profiles based on the data sets from CHAMP and GRACE between May 2001 and October 2009 for different regions and seasons. The vertical coordinate is tropopause-based.

4.1.2. Climatology

[60] A typical N^2 structure is apparent if a climatological mean from all CHAMP and GRACE RO profiles is established. Figure 7 shows mean N^2 profiles for the NH and Southern Hemisphere (SH) extratropics (40°–60° and 60°–90°) as well as for the deep tropics (10°N–10°S) for December–February (DJF) and June–August (JJA). The transition zone between the deep tropics and the midlatitudes (10°–40°) is also shown.

[61] For the midlatitude and polar regions on both hemispheres, the N^2 profiles exhibit the same structure independent from season with the three distinctive points already mentioned above: a local minimum 1–2 km below the LRT (closer to the LRT during summer), a maximum within 1 km above the LRT, and a local minimum 3–4 km above the LRT.

[62] It is evident from Figure 7 that the strongest TIL occurs during the polar summer period [*Randel et al.*, 2007; *Grise et al.*, 2010; *Randel and Wu*, 2010] and it is also known that the polar winter LRT is often not defined and therefore the TIL do not exist [*Tomikawa and Yamanouchi*, 2010].

[63] Beside the qualitative agreement of the midlatitude and polar TIL structure there are quantitative differences. The most noticeable is the stronger TIL (N^2 maximum) during the summer compared with the winter season. This effect is much better pronounced for the polar region and for the NH. For the extratropics the TIL maximum height is slightly higher in summer than in winter. In contrast, the SH midlatitude region exhibits nearly the same height of the N^2 maximum.

[64] For the tropics the mean N^2 maximum is little higher compared with the extratropical profiles and located 100–200 m above the extratropical maximum. In the mean tropical N^2 profiles, there is no difference between the maximum height in summer and winter. The minimum below the tropopause is about 2 km lower compared with the extratropics. A local minimum above the tropopause, equivalent to the extratropics, is not observed in the mean N^2 profile.

[65] It should be noted that between 10° and 40° on both hemispheres a second N^2 maximum is slightly indicated about 2 km above the LRT. This is in agreement with *Grise et al.* [2010]. They report also a second N^2 maximum in the tropics based on CHAMP data, but for the latitude bands 10°N–20°N and 10°S–20°S.

[66] Because the MOZAIC data focus to the latitude band between 40°N and 60°N, Figure 8 presents the mean seasonal N^2 profiles from CHAMP and GRACE for that region in more detail. Additional to Figure 7 the results for the time periods MAM and September–November (SON) are shown. The shaded area indicate the interval between the mean TIL bottom (N^2 minimum below the LRT) and TIL top (temperature maximum above the LRT) heights. Both heights are located about 2 km below/above the LRT (Table 2).

[67] It should be noted that for the NH midlatitudes (40°N–60°N) a seasonal cycle of TIL bottom and TIL top heights is observed with closest values to the LRT during summer. An similar cycle over the complete extratropics (40°N–90°N) is only observed for the TIL bottom height, but not for the TIL top. The extratropical TIL maximum height is highest in spring (Table 2).

4.1.3. Seasonal Variation

[68] Figure 9 shows the global TIL structure as an altitude-latitude section for different seasons. CHAMP/GRACE N^2 is plotted in LRT-based coordinates for 5° latitude bands from 90°N–90°S.

[69] In contrast to *Birner* [2006] and *Grise et al.* [2010], we adjust the altitude in Figure 9 at the LRT level and use not the modified altitude adjusted at the mean LRT because we want to be consistent with the following MOZAIC presentations. The LRT-based coordinates used here allow an easier comparison of different mean profiles from different seasons, because the mean LRT changes with season.

4.1.3.1. TIL Bottom Height

[70] The TIL bottom height as proposed by *Hegglin et al.* [2009] is the height of the N^2 minimum below the LRT. Generally, the extratropical (40°–90°) TIL bottom height is

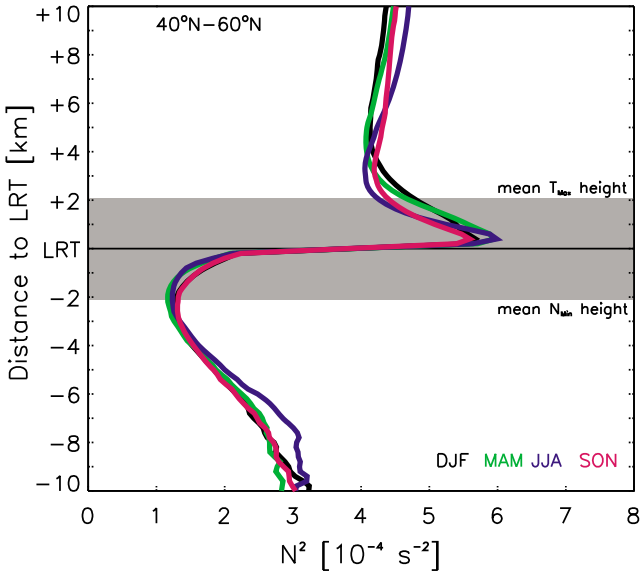

Figure 8. Mean N^2 profiles based on the data sets from CHAMP and GRACE between May 2001 and October 2009 for the Northern Hemisphere midlatitudes (40°N–60°N). The vertical coordinate is tropopause-based. The bottom of the shaded area denotes the mean height of N^2_{Min} below the tropopause. The top of the shaded area denotes the mean height of the temperature maximum above the tropopause.

closer to the LRT in summer than in winter (Figure 9). The mean difference is about 0.9 km for the NH and 1.2 km for the SH. The higher difference for the SH is caused by the lower mean TIL bottom height during winter (JJA) at the SH (Figure 9c) compared with the NH. For the NH midlatitudes (40°N–60°N) the difference between winter and summer is only 0.4 km.

[71] The difference between the NH and SH extratropical TIL bottom height during summer is about 0.2 km, whereas the hemispheric difference between TIL bottom during winter is about 0.5 km. The lowest values of the extratropical TIL bottom are found in the SH polar region during winter (June–August) and the breakdown of the polar vortex (September–November).

[72] In the subtropics and tropics (40°N–40°S) during December–May (Figures 9a and 9b) the TIL bottom height has a typical W-shaped form with nearly constant heights. This structure is maintained from June to November between the tropics and the SH subtropics, whereas the TIL bottom height in the NH subtropics is increased during summer (Figure 9c) compared with the SH. A possible reason for this behavior could be the variation (in strength and location) of the subtropical jet stream, which is much more variable on the NH compared with the SH [*Holton*, 2004].

[73] Later we will discuss the linkage between the NH midlatitude TIL bottom height and the tropospheric ozone gradient structure.

4.1.3.2. TIL Maximum Height

[74] The TIL maximum height defined here as the altitude of the N^2 maximum above the LRT is nearly constant in the extratropics of both hemispheres. The only exception occurs in the SH polar region during the occurrence (June–August) and breakdown (September–November) of the polar vortex (Figures 9c and 9d) where the maximum height of N^2 is outside the LRT+10 km range considered here. It should be noted that the determination of the LRT in high latitudes during winter is generally difficult [*Highwood et al.*, 2000].

[75] The mean extratropical TIL maximum height during all seasons varies within a range of 0.5 km (NH midlatitudes) and 0.7 km (NH extratropics) above the LRT.

Table 2. Different TIL Heights From GPS RO and MOZAIC Data for Different Latitude Bands and Based on Different Methods

	GPS RO 40°S–90°S	GPS RO 40°N–90°N	GPS RO 40°N–60°N	MOZAIC (N^2) 40°N–60°N	MOZAIC (O_3) 40°N–60°N	MOZAIC (CO) 40°N–60°N
			DJF			
TIL top	2.51 ± 0.65	2.20 ± 0.25	2.34 ± 0.22	2.25 ± 1.01	-	-
TIL maximum	0.59 ± 0.15	0.61 ± 0.35	0.50 ± 0.08	0.78 ± 0.44	-	0.69 ± 0.57
TIL bottom	−1.72 ± 0.35	−2.46 ± 0.26	−2.25 ± 0.25	−2.18 ± 1.11	−1.78 ± 0.65	-
			MAM			
TIL top	2.20 ± 0.24	2.56 ± 0.23	2.27 ± 0.26	2.02 ± 0.98	-	-
TIL maximum	0.61 ± 0.11	0.70 ± 0.24	0.50 ± 0.10	0.75 ± 0.44	-	0.69 ± 0.52
TIL bottom	−1.99 ± 0.18	−1.92 ± 0.16	−1.95 ± 0.19	−2.25 ± 1.03	−2.11 ± 0.71	-
			JJA			
TIL top	1.36 ± 0.79	2.24 ± 0.41	1.87 ± 0.21	1.71 ± 0.59	-	-
TIL maximum	0.58 ± 0.22	0.63 ± 0.11	0.52 ± 0.07	0.68 ± 0.38	-	0.53 ± 0.41
TIL bottom	−2.92 ± 0.64	−1.57 ± 0.41	−1.85 ± 0.50	−2.03 ± 1.02	−2.21 ± 0.67	-
			SON			
TIL top	1.46 ± 0.59	2.22 ± 0.35	1.90 ± 0.23	1.70 ± 0.79	-	-
TIL maximum	-	0.68 ± 0.19	0.52 ± 0.09	0.72 ± 0.41	-	0.56 ± 0.48
TIL bottom	−2.77 ± 0.53	−2.22 ± 0.33	−2.25 ± 0.47	−2.21 ± 1.07	−1.80 ± 0.57	-
			All Seasons			
TIL top			2.10 ± 0.23	1.93 ± 0.84	-	-
TIL maximum			0.52 ± 0.10	0.73 ± 0.42	-	0.65 ± 0.53
TIL bottom			−2.08 ± 0.35	−2.17 ± 1.06	−1.90 ± 0.65	-

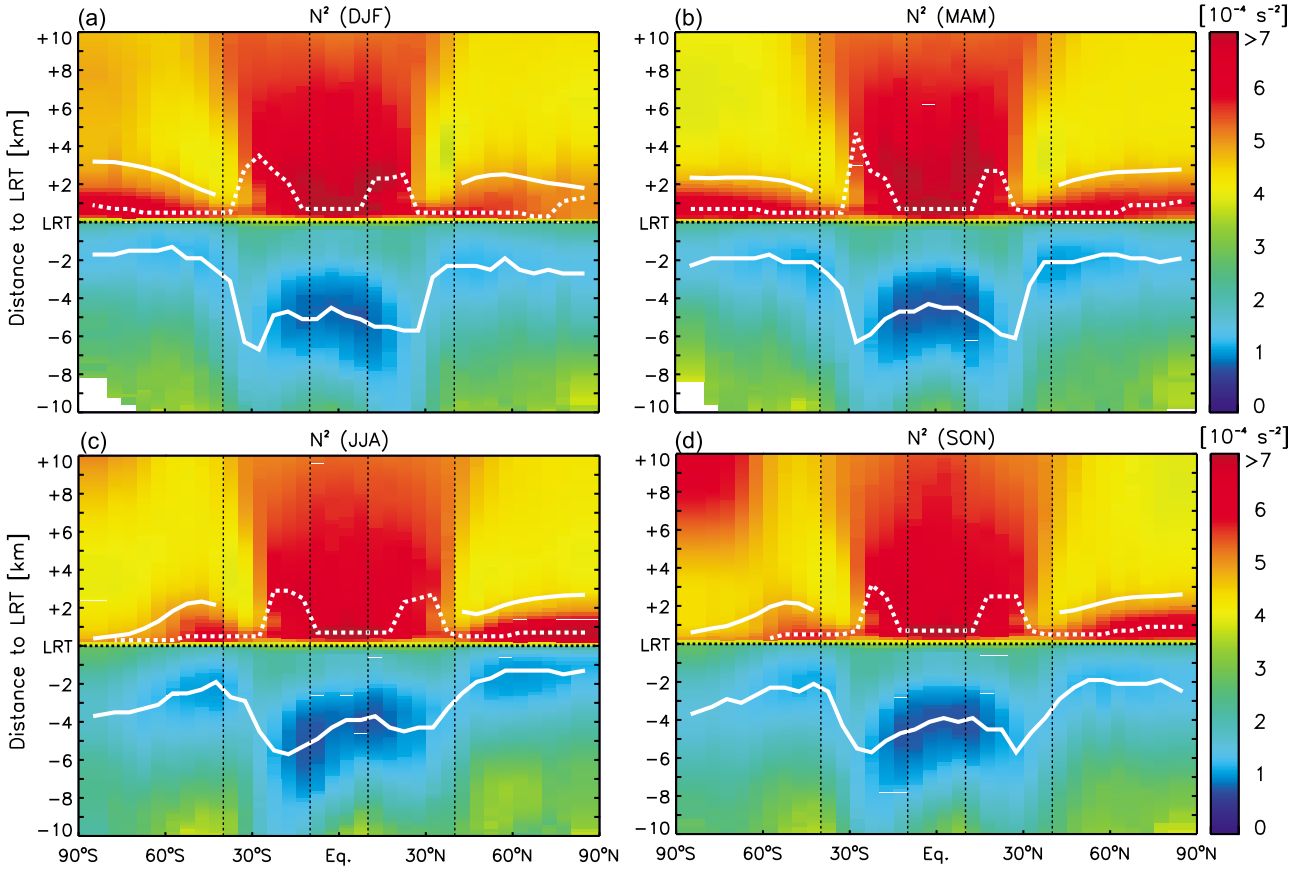

Figure 9. Zonal mean N^2 ± 10 km around the thermal tropopause (LRT) for seasons (a) DJF, (b) MAM, (c) JJA, and (d) SON derived from the CHAMP and GRACE data sets (2001–2009). The dotted white lines show the N^2 maximum above the LRT, and the solid white lines denote the height of the temperature maximum above the LRT and the height of the N^2 minimum below the LRT.

[76] A similar constant N^2 maximum height is also present in the deep tropics (10°N–10°S) with a slightly higher altitude (100–200 m) compared with the extratropics (see also Figure 7).

[77] In the subtropics (10°–40°) on both hemispheres the situation is different. There is no constant N^2 maximum height, but a continuous increase of the N^2 maximum height from the deep tropical side (10° on both hemispheres) up to the maximum between 20° and 30°. The reason is the double maximum structure of N^2 in that region with a second maximum 2–3 km above the LRT (Figure 7). With the meridional resolution of 5 deg used in Figure 9 the double maximum structure of N^2 is better emerged.

[78] We will also show later the correlation of the NH midlatitude TIL maximum height with the carbon monoxide gradient structure just above the LRT.

4.1.3.3. TIL Top Height

[79] During all seasons enhanced N^2 values exist in the NH and SH extratropics (40°–90°) in a layer 1–3 km above the LRT. The top of this layer can be quantified by the height of the temperature maximum above the LRT (not shown here). The white solid line in Figure 9 above the LRT mark this altitude and is called the TIL top height here.

[80] The mean NH extratropical TIL top height varies between 2.2 km and 2.6 km above the LRT, whereas the SH TIL top height span a larger range from 1.4 km during winter and 2.5 km during summer. The lowest values occur within the polar vortex and reach nearly the LRT at the pole (Figures 9c and 9d).

[81] Further on we demonstrate that the NH midlatitude TIL top height is related to the carbon monoxide gradient structure.

[82] A statistic of the different extratropical (NH midlatitude) TIL heights from GPS RO data is summarized in Table 2.

4.2. MOZAIC

[83] The NH seasonal mean N^2 profiles derived from the MOZAIC temperature data are presented in Figure 10 separated for cases including thermal tropopauses only for the strong WMO criterion (Figure 10a) and the modified version (Figure 10b). For the statistics only measurements with at least 50 measurements per altitude bin (150 m vertical resolution) were considered.

[84] The differences between the data sets using the strong and modified tropopause definition are marginal. The modified WMO version gives smoother tropospheric values and the standard deviation between the different seasons is closer. The mean TIL bottom height is nearly unaffected, but the TIL top height between the different tropopause versions

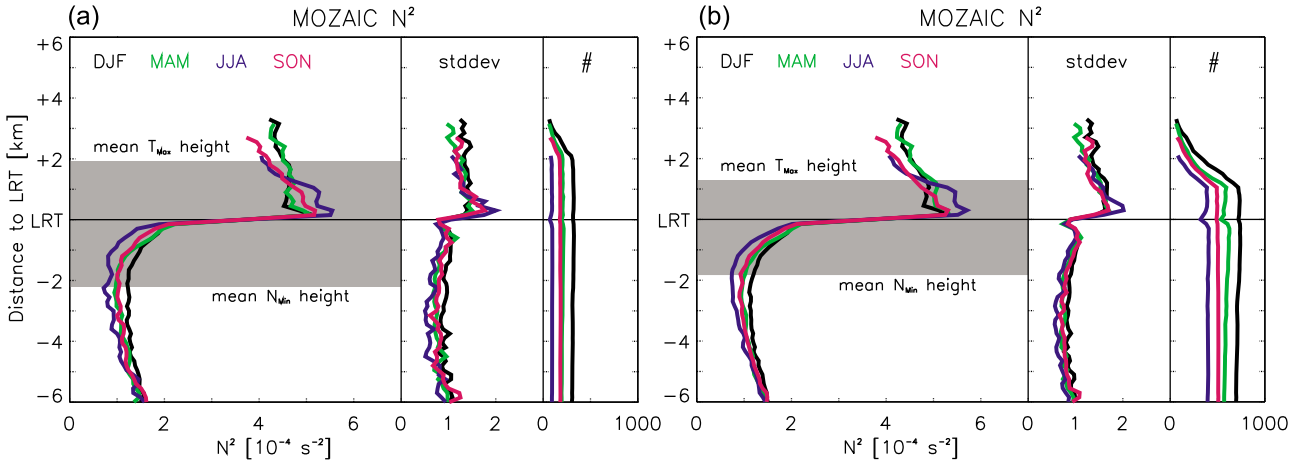

Figure 10. (a) Mean N^2 of the MOZAIC data for the Northern Hemisphere midlatitudes (40°N–60°N) and (left) different seasons, (middle) the standard deviation, and (right) the number of profiles. (b) Same as Figure 10a but for the modified WMO tropopause definition. The bottom of the shaded area denotes the mean height of N^2_{Min} below the tropopause. The top of the shaded area denotes the mean height of the temperature maximum above the tropopause.

differs of about 0.6 km with the lower value for the statistic includes also profiles with modified tropopauses. This is expected because the temperature maximum above the LRT in that cases is only searched up to an altitude of LRT+1 km.

[85] A comparison with the CHAMP/GRACE data set based on the time interval 2001–2009 (Figure 8) shows also no basic differences in the characteristics of the mean profiles, even the TIL bottom and TIL maximum heights agree very well. The latter is a further indication that there is no basic difference in the N^2 structure between mostly cyclonic (MOZAIC data) and cyclonic plus anticyclonic (GPS RO data) situations.

[86] Differences between GPS RO and MOZAIC N^2 data occur in the upper troposphere with $N^2_{MOZAIC} < N^2_{GPSRO}$. The variations can be addressed to the nonconsideration of water vapor in the RO retrieval (equation (2)). Using "dry temperatures" in equation (3) leads to larger N^2 values compared with "real temperatures."

[87] The TIL top heights deduced from MOZAIC (Table 2) exhibit a similar seasonal cycle compared to GPS RO data with highest TIL top heights during winter (2.25 km above LRT) and lowest values during summer (1.71 km) and fall (1.70 km).

[88] The TIL bottom heights are also closest to the LRT in summer compared with the other seasons.

5. Trace Gas Measurements From MOZAIC

5.1. Seasonal Means

[89] Measurements of trace gases (e.g., O_3, CO, H_2O) are usually used to characterize and quantify the exchange between the troposphere and stratosphere and vice versa. An efficient tool for the determination of the chemical transition across the tropopause is the tracer-tracer correlation between a tropospheric and a stratospheric species. Mostly the H_2O-O_3 and/or the CO-O_3 correlations are applied [*Hoor et al.*, 2002; *Pan et al.*, 2004, 2007; *Hegglin et al.*, 2009].

[90] Figures 11a and 11b show seasonal mean profiles of ozone, and carbon monoxide mixing ratios in the vicinity of the tropopause. One can clearly see that ozone dominates in the lower stratosphere (stratospheric tracer) whereas carbon monoxide prevail in the troposphere (tropospheric tracer).

[91] The goal of this study is to search for relations between the TIL structure in the MOZAIC trace gas profiles according to Figures 8 and 10 and to confirm the results with respect to consider the TIL as a mixing layer.

[92] The importance of the tropopause as a separator for the concentrations of O_3 and CO is evident (Figures 11a and 11b), but the permanent presence of the TIL is only rudimental visible.

[93] An unique way to detect the TIL structure in trace gas measurements is the usage of trace gas mixing ratio gradients [*Hegglin et al.*, 2009]. Figures 11c and 11d illustrate the seasonal mean values of O_3 and CO mixing ratio gradients representing the means over all individual profiles. Some interesting features are: (1) the absolute maxima of the O_3 and CO mixing ratio gradients are located at the LRT, (2) below the TIL bottom height (~2 km below the LRT) the mean mixing ratio gradients of O_3 is nearly constant with values of about 0–5 ppbv/km, and (3) within 1 km above the LRT the mean CO mixing ratio gradients increase very fast. Considering properties 2 and 3, threshold values will be defined to reproduce the TIL maximum and the TIL bottom heights from individual trace gas mixing ratio gradient profiles.

[94] On the other hand, due to the excellent agreement between the mean heights of the maximum and minimum mixing ratio gradients of O_3 and CO with the LRT, an attempt is made to deduce trace gas tropopause heights from individual ozone and carbon monoxide mixing ratio gradient profiles as well.

5.2. LRT Height From O_3 and CO Mixing Ratio Gradients

[95] For the tropopause several definitions have been introduced. By using the lapse rate criterion the thermal tropopause is given, the potential vorticity [*Holton*, 2004] is used to define the dynamical tropopause, whereas ozone

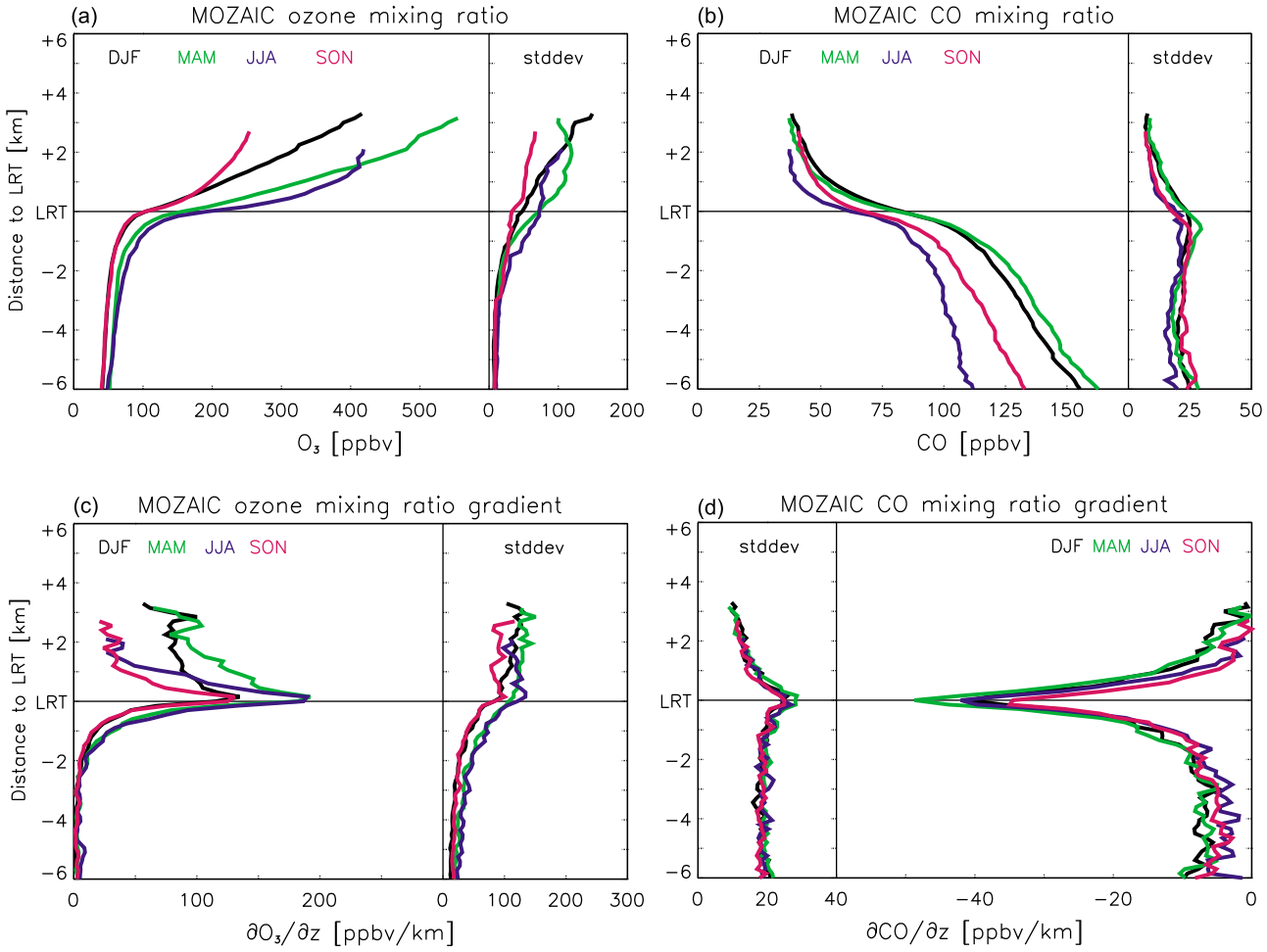

Figure 11. Seasonal mean profiles and standard deviation of MOZAIC trace gases mixing ratios in a tropopause-based coordinate system for the Northern Hemisphere midlatitudes (40°N–60°N): (a) ozone (May 2001 to December 2008) and (b) carbon monoxide (January 2002 to December 2008) and (c, d) appropriate mixing ratio gradients. For the statistic, only altitude bins with at least 50 data points were considered.

mixing ratios can also serve to define the tropopause level (ozonopause). The choice of the tropopause definition depends on the question, what is to be examined [*Pan et al.*, 2004].

[96] *Bethan et al.* [1996] suggested a formalism to determine the ozonopause from O_3 profiles and found the ozonopause on average 800 m below the LRT. Applying the definition from *Bethan et al.* [1996] to the MOZAIC ozone data the mean MOZAIC ozonopause is about 620 m below the LRT (Figure 12). The ozonopause after *Bethan et al.* [1996] is defined in terms of both the mixing ratio and the mixing ratio gradients of ozone. *Bethan et al.* [1996] found most of the ozonpauses above the thermal tropopause linked to anticyclonic flow. The majority of the MOZAIC ozonopauses are below the LRT (Figure 12). This seems to be in agreement with the results from *Bethan et al.* [1996] because the MOZAIC data are mostly available under cyclonic conditions.

[97] In this study we define an ozone tropopause height (TPH_{Ozone}) only based on the height of the maximum mixing ratio gradient. An according carbon monoxide tro-

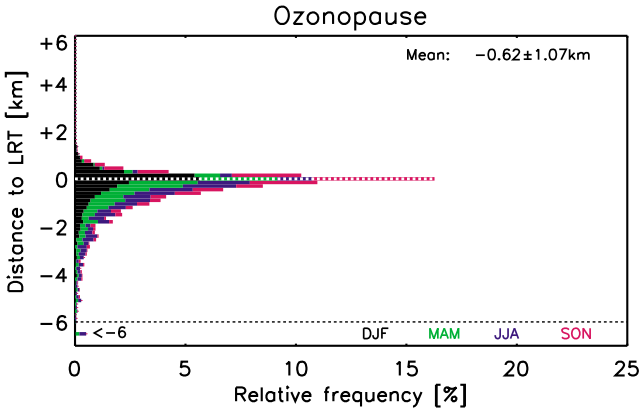

Figure 12. Relative frequency histogram of MOZAIC ozonopauses [*Bethan et al.*, 1996] related to the LRT for different seasons based on the time period 2001–2008.

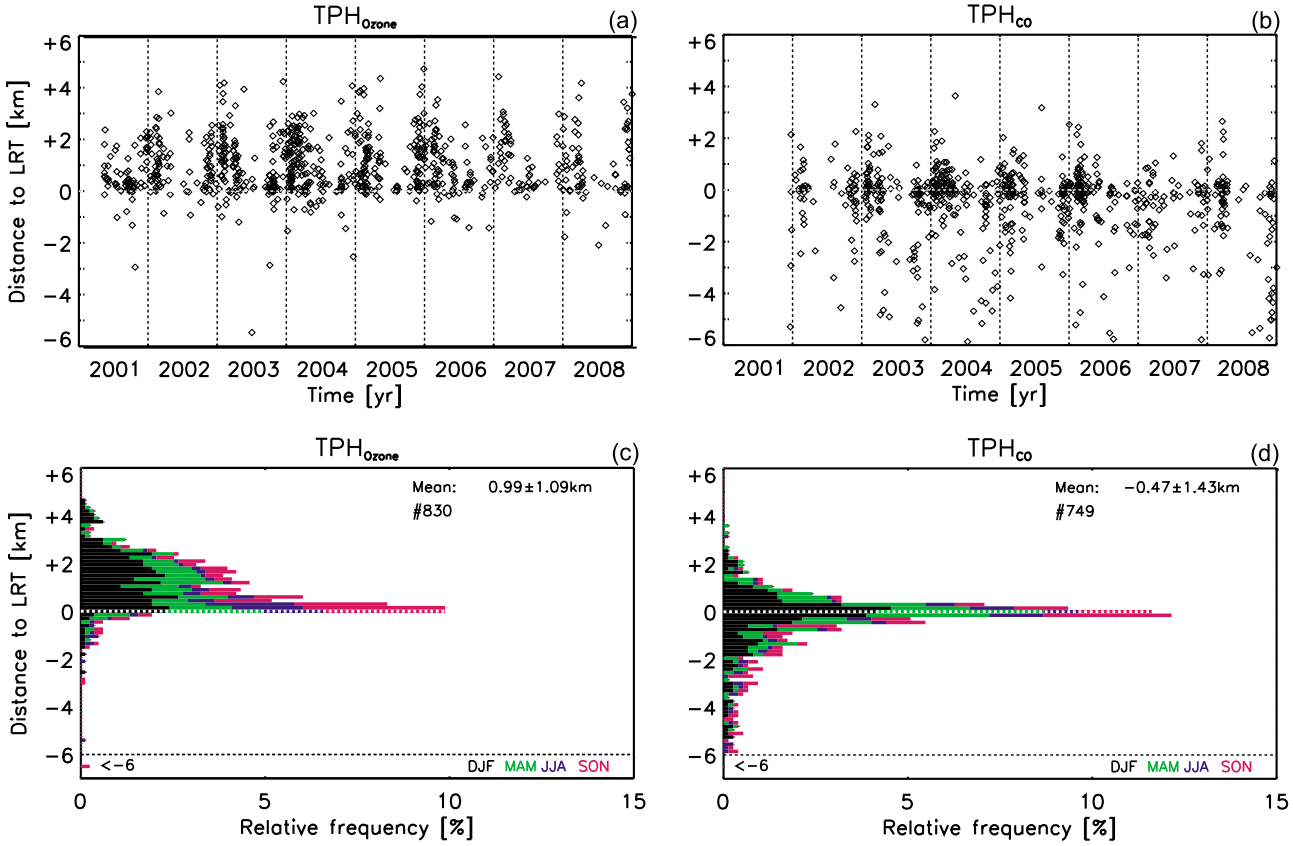

Figure 13. (a) Time series of individual ozone tropopause heights (TPH_{Ozone}) relative to LRT heights from MOZAIC measurements. (b) Same as Figure 13a but for carbon monoxide tropopause heights (TPH_{CO}). (c) Relative frequency histogram of TPH_{Ozone} related to the LRT based on the data from Figure 13a. (d) Same as Figure 13c but for TPH_{CO} based on the data from Figure 13b.

popause height (TPH_{CO}) is defined at the height of the minimum mixing ratio gradient.

[98] In Figures 13a and 13b time series of TPH_{Ozone} and TPH_{CO} for each individual MOZAIC profile relative to the LRT are presented. Histogram plots of the relative frequency distribution of the individual trace gas tropopauses relative to the LRT are shown in Figures 13c and 13d.

[99] The relative frequency distribution of TPH_{Ozone} exhibits a maximum at the LRT, but there is also a large fraction of profiles that have their maximum in a layer between 1 and 3 km above the LRT. This is an interesting fact because the TIL top height derived from N^2 profiles is at about 2 km above the LRT (Table 2). One can also recognize the O_3 gradient enhancement in that layer in the seasonal means for DJF and MAM (Figure 11c).

[100] For TPH_{CO} the results are similar with also a maximum of the relative frequency distribution around the LRT that follows more a Gaussian distribution compared with TPH_{Ozone}. In contrast to the ozone profiles there is no dominant fraction of CO profiles reaching their gradient maximum higher than 1 km above the thermal tropopause.

[101] The highest absolute gradients around the LRT demonstrate that both tracers (CO and O_3) have experienced a rapid change across the LRT, indicating that the thermal tropopause is a chemical boundary between the troposphere and stratosphere [*Pan et al.*, 2004]. As proposed by *Randel et al.* [2007] the vertical scale of the TIL (inversion) could be linked to the thickness of the chemical transition layer. This will be a topic of further investigation.

[102] It should be noted that a very good agreement between the height of the minimum of CO mixing ratio gradients with the LRT was also reported by *Hegglin et al.* [2009, Figure 13].

5.3. TIL Heights

[103] Based on the results of the seasonal mean O_3 and CO mixing ratio gradients (Figures 11c and 11d) threshold values for the identification of the TIL bottom and the TIL maximum height from individual trace gas mixing ratio gradient profiles are determined.

[104] The idea is to use the gradient of a tropospheric tracer (CO) to determine the TIL maximum and TIL top height and the gradient of a stratospheric tracer (O_3) for the determination of the TIL bottom. This could be a method for the identification of the TIL as a mixing layer around the LRT.

[105] The following criteria are established using O_3 and CO mixing ratio gradients: (1) the TIL bottom height from an ozone mixing ratio gradient profile is defined at the lowest level below the LRT where the mean gradient is $\partial O_3/\partial z > 40$ ppbv/km over an altitude range of 2 km above that level and (2) the TIL maximum height is identified from a

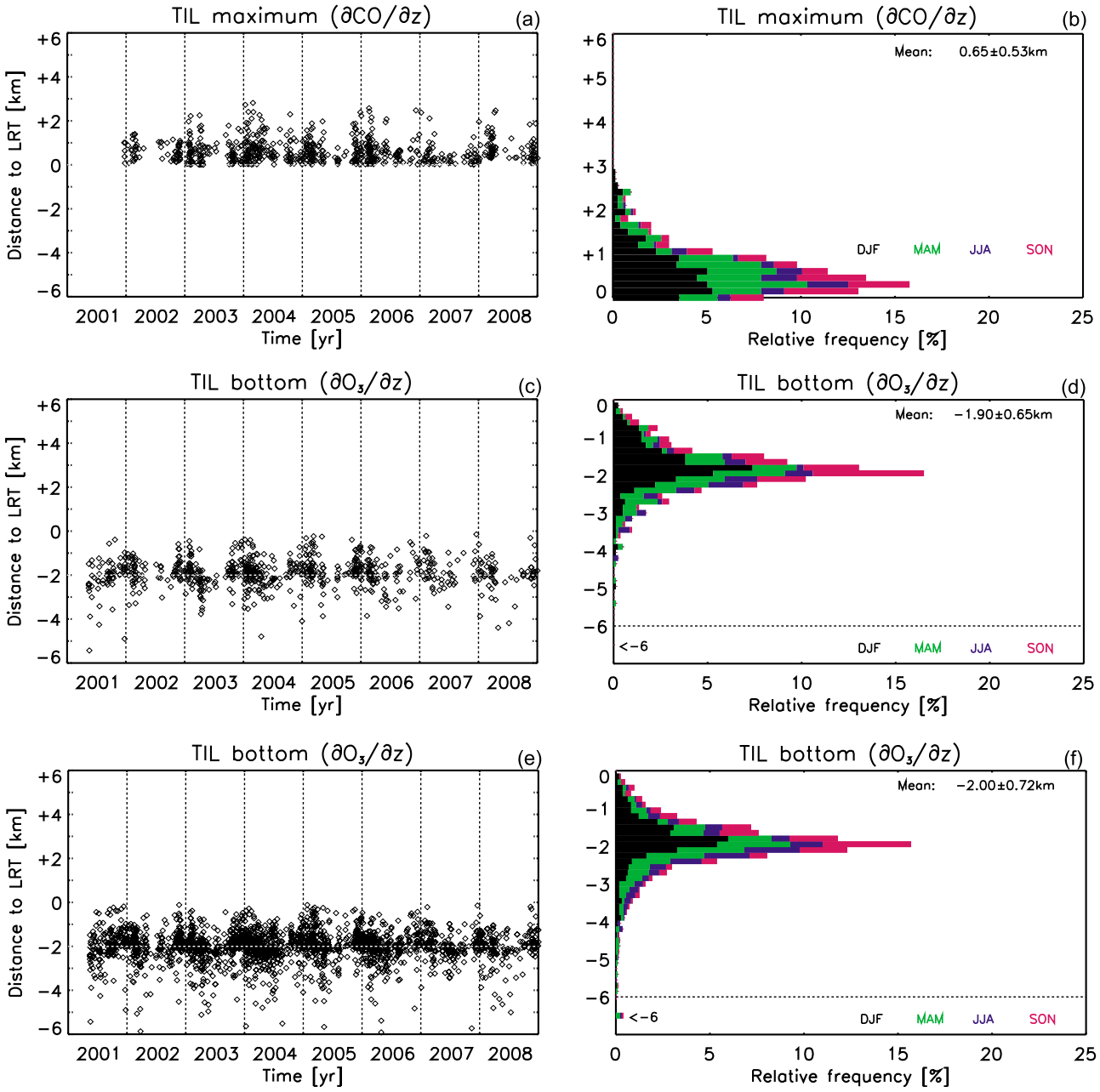

Figure 14. (a) Time series of individual TIL maximum heights relative to LRT heights from MOZAIC measurements. (b) Relative frequency histogram relating to Figure 14a for different seasons. (c) Time series of individual TIL bottom heights relative to LRT heights from MOZAIC measurements. (d) Relative frequency histogram relating to Figure 14c for different seasons. (e, f) Same as Figures 14c and 14d but for LRT heights after the modified WMO criterion.

carbon monoxide mixing ratio gradient at the first level above the LRT where the absolute gradient $\partial CO/\partial z$ is less than 25% of the absolute maximum value near the LRT.

[106] Both threshold values are the empirical best values by comparing the TIL bottom and TIL maximum height derived from N^2 with $\partial O_3/\partial z$ and $\partial CO/\partial z$, respectively. A direct definition of a TIL top height from MOZAIC CO gradients is difficult, because the last data points are statistically not high enough.

[107] In the following we will keep the introduced nomenclature TIL bottom, TIL maximum and TIL top height to name also the tracer gradient inflection points, although the tracer behaviors mark the chemical gradient change and not the thermal inversion layer. Nevertheless, the shown relationship between the tracer gradients and the TIL structure might justify this naming.

[108] The threshold values (40 ppbv/km) for O_3 mixing ratio gradients and the 25% criterion for the decrease of CO gradients in relation to the absolute maximum value reflect the significantly change of ozone and carbon monoxide from the troposphere to the lower stratosphere (Figures 11a and 11b).

[109] Figures 14a and 14b presents the TIL maximum heights (time series and histograms) using CO mixing ratio gradients (criterion 2 above). The peak in the relative frequency distribution are located around 0.5 km (mean 0.65 km) which is a good approximation of the TIL maximum height deduced from N^2 profiles (0.73 km; Table 2).

[110] The application of the threshold value for O_3 mixing ratio gradients (Figures 14c and 14d) for the identification of the TIL bottom height (1.9 km below the LRT) is in good agreement with the height of the local N^2 minimum below the tropopause (2.17 km below the LRT; Table 2).

[111] Figures 14e and 14f present the same results as Figures 14c and 14d, but for the inclusion of profiles which tropopauses have been determined with the modified WMO criterion. As one can see there is no significant difference between both data sets if only data below the LRT are considered.

[112] Generally, the reproduction of the TIL maximum height with trace gas measurements from MOZAIC is more complicated compared with the TIL bottom or trace gas tropopause height because only a small amount of profiles extends significantly above the LRT (>2 km or more).

[113] The TIL top height based on MOZAIC CO gradients can be, if at all, only determined indirectly. Considering Figure 14b the height were nearly all profiles below 25% of the absolute CO gradient maximum value is at about 2 km above the LRT. This is just the height were the TIL top is found from the temperature maximum height above the LRT (1.93 km; Table 2).

[114] The TIL bottom heights deduced from MOZAIC ozone gradients (Table 2) exhibit a slightly seasonal cycle with values farther from the LRT during summer (2.21 km below the LRT) than during winter (1.78 km below the LRT). This is contrary to the annual cycle of the TIL bottom heights derived from N^2, but the mean TIL bottom values over all seasons derived from N^2 (GPS RO and MOZAIC) as well as from O_3 gradients differ only by 300 m.

[115] In the context that the TIL could be considered as a mixing layer around the tropopause (not only above) the seasonal cycle of the TIL bottom height based on O_3 gradients might be an indicator for a more expanded NH midlatitude TIL and/or mixing layer into the troposphere during summer compared with winter and will be topic for a following study.

6. Summary

[116] In this study we have investigated two different data sets with the goal to identify on the one hand the TIL structure in both data sets using N^2 profiles. Temperature profiles from GPS RO data from CHAMP and GRACE and high-resolution aircraft measurements (MOZAIC) were used to analyze the NH midlatitude TIL bottom, TIL maximum and TIL top height. Additionally, in situ trace gas profile measurements (O_3 and CO) from the MOZAIC program were used as complementary data sets showing most of the TIL structure if the mixing ratio gradients of the trace gas measurements were exploit.

[117] The NH midlatitude TIL top heights relative to the LRT derived from MOZAIC and GPS RO data show a seasonal cycle with highest values during winter and lowest values during summer and fall. The TIL bottom heights are closest to the LRT in summer compared with the other seasons.

[118] By using mixing ratio gradients of the individual MOZAIC trace gas profiles we could also demonstrate, that at least in a climatological sense, the LRT height is strongly correlated with the height of the absolute maxima of ozone and carbon monoxide mixing ratio gradients and generally high gradients within the TIL.

[119] We have used ozone gradients (stratospheric tracer) to identify the TIL bottom height (located in the troposphere) and carbon monoxide gradients (tropospheric tracer) to identify the TIL maximum height (located in the stratosphere) by introduction of typical threshold values for the mixing ratio gradients. We could show on a climatological basis that these TIL heights derived from the trace gas mixing ratio gradients are in good agreement with the TIL structure deduced from N^2 (temperature).

[120] The qualitatively, but also quantitatively, good agreement of the different TIL heights deduced on the one hand from temperature and/or N^2 profiles and on the other hand determined from the vertical structure of O_3 and CO gradients could be indicators for the radiative-based explanation of the TIL maintenance.

[121] Because the flight ceiling of the commercial aircrafts between 9 and 12 km the MOZAIC data are dominated by relatively low tropopauses which are mainly associated with cyclonic conditions or upper level troughs. The analysis of relative vorticity at 200 hPa has shown this fact very clear. Therefore the results and conclusions presented here should be interpreted in that manner.

[122] **Acknowledgments.** The authors would like to thank the other members of the CHAMP and GRACE team at GFZ Potsdam working with RO data and providing the orbits. The authors acknowledge the strong support of the European Commission, Airbus, and the airlines (Lufthansa, Austrian, Air France, and Air Namibia) that carry free of charge the MOZAIC equipment and have performed the maintenance since 1994. MOZAIC is presently funded by INSU-CNRS (France), Meteo-France, and Research Centre Jülich (Germany). The MOZAIC database is supported by ETHER (CNES and INSU-CNRS). Further, the authors thank ECMWF for the provision of operational ananlyses and the ERA interim data. Finally, the authors thank the three anonymous reviewers for their constructive comments and suggestions which helped to improve the article.

References

Andrews, D. G., J. R. Holton, and C. B. Leovy (1987), *Middle Atmosphere Dynamics*, *Int. Geophys. Ser.*, vol. 40, Academic, San Diego, Calif.

Bethan, S., G. Vaughan, and S. J. Reid (1996), A comparison of ozone and thermal tropopause heights and the impact of tropopause definition on quantifying the ozone content of the troposphere, *Q. J. R. Meteorol. Soc.*, *122*, 929–944.

Birner, T. (2006), Fine-scale structure of the extratropical tropopause region, *J. Geophys. Res.*, *111*, D04104, doi:10.1029/2005JD006301.

Birner, T., D. Sankey, and T. G. Shepherd (2006), The tropopause inversion layer in models and analyses, *Geophys. Res. Lett.*, *33*, L14804, doi:10.1029/2006GL026549.

Borsche, M., G. Kirchengast, and U. Foelsche (2007), Tropical tropopause climatology as observed with radio occultation measurements from CHAMP compared to ECMWF and NCEP analyses, *Geophys. Res. Lett.*, *34*, L03702, doi:10.1029/2006GL027918.

Brioude, J., J.-P. Cammas, O. R. Cooper, and P. Nedelec (2008), Characterization of the composition, structure, and seasonal variation of the mixing layer above the extratropical tropopause as revealed by MOZAIC measurements, *J. Geophys. Res.*, *113*, D00B01, doi:10.1029/2007JD009184.

Gobiet, A., G. Kirchengast, G. L. Manney, M. Borsche, M. Retscher, and G. Stiller (2007), Retrieval of temperature profiles from CHAMP for cli-

mate monitoring: Intercomparison with Envisat MIPAS and GOMOS and different atmospheric analyses, *Atmos. Chem. Phys.*, *7*, 3519–3536.
Grise, K. M., D. W. J. Thompson, and T. Birner (2010), A global survey of static stability, *J. Clim.*, *23*, 2275–2292, doi:10.1175/2009JCLI3369.1.
Hajj, G. A., C. O. Ao, B. A. Iijima, D. Kuang, E. R. Kursinski, A. J. Mannucci, T. K. Meehan, L. J. Romans, M. de la Torre Juarez, and T. P. Yunck (2004), CHAMP and SAC-C atmospheric occultation results and intercomparisons, *J. Geophys. Res.*, *109*, D06109, doi:10.1029/2003JD003909.
Hegglin, M. I., C. D. Boone, G. L. Manney, and K. A. Walker (2009), A global view of the extratropical tropopause transition layer from Atmospheric Chemistry Experiment Fourier Transform Spectrometer O_3, H_2O, and CO, *J. Geophys. Res.*, *114*, D00B11, doi:10.1029/2008JD009984.
Heise, S., J. Wickert, G. Beyerle, T. Schmidt, H. Smit, J.-P. Cammas, and M. Rothacher (2008), Comparison of water vapour and temperature results from GPS radio occultation aboard CHAMP with MOZAIC aircraft measurements, *IEEE Trans. Geosci. Remote Sens.*, *46*(11), 3406–3411, doi:10.1109/TGRS.2008.920268.
Helten, M., H. G. J. Smit, W. Sträter, D. Kley, P. Nedelec, M. Zöger, and R. Busen (1998), Calibration and performance of automatic compact instrumentation for the measurement of relative humidity from passenger aircraft, *J. Geophys. Res.*, *103*(D19), 25,643–25,652, doi:10.1029/98JD00536.
Highwood, E. J., B. J. Hoskins, and P. Berrisford (2000), Properties of the Arctic tropopause, *Q. J. R. Meteorol. Soc.*, *126*, 1515–1532.
Holton, J. R. (2004), *An Introduction to Dynamic Meteorology*, Academic, San Diego, Calif.
Holton, J. R., P. H. Haynes, M. E. McIntyre, A. R. Douglass, R. B. Rood, and L. Pfister (1995), Stratosphere-troposphere exchange, *Rev. Geophys.*, *33*(4), 403–439, doi:10.1029/95RG02097.
Hoor, P., H. Fischer, L. Lange, J. Lelieveld, and D. Brunner (2002), Seasonal variations of a mixing layer in the lowermost stratosphere as identified by the CO-O_3 correlation from in situ measurements, *J. Geophys. Res.*, *107*(D5), 4044, doi:10.1029/2000JD000289.
Kunz, M. I., P. Konopka, R. Müller, L. L. Pan, C. Schiller, and F. Rohrer (2009), High static stability in the mixing layer above the extratropical Tropopause, *J. Geophys. Res.*, *114*, D16305, doi:10.1029/2009JD011840.
Kuo, Y.-H., W. S. Schreiner, J. Wang, D. L. Rossiter, and Y. Zhang (2005), Comparison of GPS radio occultation soundings with radiosondes, *Geophys. Res. Lett.*, *32*, L05817, doi:10.1029/2004GL021443.
Kursinski, E. R., G. A. Hajj, K. R. Hardy, J. T. Schofield, and R. Linfield (1997), Observing Earth's atmosphere with radio occultation measurements using the Global Positioning System, *J. Geophys. Res.*, *102*(D19), 23,429–23,465, doi:10.1029/97JD01569.
Marenco, A. et al. (1998), Measurement of ozone and water vapor by Airbus in-service aircraft: The MOZAIC airborne program, An overview, *J. Geophys. Res.*, *103*(D19), 25,631–25,642, doi:10.1029/98JD00977.
Melbourne, W. G., E. S. Davis, G. A. Hajj, K. R. Hardy, E. R. Kursinski, T. K. Meehan, and L. E. Young (1994), The application of spaceborne GPS to atmospheric limb sounding and global change monitoring, *JPL Publ.*, 94–18, 147 pp.
Nedelec, P., J.-P. Cammas, V. Thouret, G. Athier, J.-M. Cousin, C. Legrand, C. Abonnel, F. Lecoeur, G. Cayez, and C. Marizy (2003), An improved infrared carbon monoxide analyser for routine measurements aboard commercial Airbus aircraft: technical validation and first scientific results of the MOZAIC III programme, *Atmos. Chem. Phys.*, *3*, 1551–1564.
Pan, L. L., W. J. Randel, B. L. Gary, M. J. Mahoney, and E. J. Hintsa (2004), Definitions and sharpness of the extratropical tropopause: A trace gas perspective, *J. Geophys. Res.*, *109*, D23103, doi:10.1029/2004JD004982.
Pan, L. L., J. C. Wei, D. E. Kinnison, R. R. Garcia, D. J. Wuebbles, and G. P. Brasseur (2007), A set of diagnostics for evaluating chemistry-climate models in the extratropical tropopause region, *J. Geophys. Res.*, *112*, D09316, doi:10.1029/2006JD007792.
Randel, W. J., and F. Wu (2010), The polar summer tropopause inversion layer, *J. Atmos. Sci.*, *67*, 2572–2581, doi:10.1175/2010JAS3430.1.
Randel, W. J., F. Wu, and P. Forster (2007), The extratropical tropopause inversion layer: Global observations with GPS data and radiative forcing mechanism, *J. Atmos. Sci.*, *64*, 4489–4496, doi:10.1175/2007JAS2412.1.
Reichler, T., M. Dameris, and R. Sausen (2003), Determination of tropopause height from gridded data, *Geophys. Res. Lett.*, *30*(20), 2042, doi:10.1029/2003GL018240.
Schmidt, T., J. Wickert, G. Beyerle, and C. Reigber (2004), Tropical tropopause parameters derived from GPS radio occultation measurements with CHAMP, *J. Geophys. Res.*, *109*, D13105, doi:10.1029/2004JD004566.
Schmidt, T., J. Wickert, G. Beyerle, R. König, R. Galas, and C. Reigber (2005a), The CHAMP atmospheric processing system for radio occultation measurements, in *Earth Observation With CHAMP*, edited by C. Reigber et al., pp. 597–602, Springer, Berlin.
Schmidt, T., S. Heise, J. Wickert, G. Beyerle, and C. Reigber (2005b), GPS radio occultation with CHAMP and SAC-C: Global monitoring of thermal tropopause parameters, *Atmos. Chem. Phys.*, *5*, 1473–1488.
Schmidt, T., J. Wickert, S. Heise, F. Flechtner, E. Fagiolini, G. Schwarz, L. Zenner, and T. Gruber (2008), Comparison of ECMWF analyses with GPS radio occultations from CHAMP, *Ann. Geophys.*, *26*, 3225–3234.
Smith, E., and S. Weintraub (1953), The constants in the equation for atmospheric refractive index at 20 radio frequencies, *Proc. IRE*, *41*, 1035–1037.
Son, S.-W., and L. M. Polvani (2007), Dynamical formation of an extratropical tropopause inversion layer in a relatively simple general circulation model, *Geophys. Res. Lett.*, *34*, L17806, doi:10.1029/2007GL030564.
Steiner, A. K., G. Kirchengast, M. Borsche, U. Foelsche, and T. Schoenengassner (2007), A multi-year comparison of lower stratospheric temperatures from CHAMP radio occultation data with MSU/AMSU records, *J. Geophys. Res.*, *112*, D22110, doi:10.1029/2006JD008283.
Thouret, V., A. Marenco, P. Nedelec, and C. Grouhel (1998a), Ozone climatologies at 9–12 km altitude as seen by the MOZAIC airborne program between September 1994 and August 1996, *J. Geophys. Res.*, *103*(D19), 25,653–25,679.
Thouret, V., A. Marenco, J. A. Logan, P. Nedelec, and C. Grouhel (1998b), Comparisons of ozone measurements from the MOZAIC airborne program and the ozone sounding network at eight locations, *J. Geophys. Res.*, *103*(D19), 25,695–25,720.
Tomikawa, Y., and T. Yamanouchi (2010), A meridional structure of static stability and ozone vertical gradient around the tropopause in the Southern Hemisphere extratropics, *Atmos. Chem. Phys. Discuss.*, *10*, 19175–19194, doi:10.5194/acpd-10-19175-2010.
Wickert, J., et al. (2001), Atmosphere sounding by GPS radio occultation: First results from CHAMP, *Geophys. Res. Lett.*, *28*, 3263–3266.
Wickert, J., et al. (2009), GPS radio occultation: Results from CHAMP, GRACE and FORMOSAT-3/COSMIC, *Terr. Atmos. Oceanic Sci.*, *20*, 35–50, doi:10.3319/TAO.2007.12.26.01(F3C).
Wirth, V. (2001), Cyclone-anticyclone asymmetry concerning the height of the thermal and the dynamical tropopause, *J. Atmos. Sci.*, *58*, 26–37.
Wirth, V. (2003), Static stability in the extratropical tropopause region, *J. Atmos. Sci.*, *60*, 1395–1409.
Wirth, V., and T. Szabo (2007), Sharpness of the extratropical tropopause in baroclinic life cycle experiments. *Geophys. Res. Lett.*, *34*, L02809, doi:10.1029/2006GL028369.
World Meteorological Organization (1957), Definition of the tropopause, *WMO Bull. 6*, 136 pp., Geneva.

J.-P. Cammas, Laboratoire d'Aerologie, Observatoire Midi-Pyrénées, CNRS, 14 Ave. Edouard Belin, F-31400 Toulouse, France.
A. Haser, S. Heise, T. Schmidt, and J. Wickert, Helmholtz Centre Potsdam, GFZ German Research Centre for Geosciences, Section 1.1: GPS/Galileo Earth Observation, Telegrafenberg A17, D-14473 Potsdam, Germany. (tschmidt@gfz-potsdam.de)
H. G. J. Smit, Institute for Energy and Climate Research: Troposphere, Research Centre Jülich, D-52425 Jülich, Germany.